

# Band structure and unconventional electronic topology of CoSi

D.A. Pshenay-Severin,<sup>1</sup> Yu.V. Ivanov,<sup>1</sup> A.A. Burkov,<sup>2</sup> and A.T. Burkov<sup>1</sup>

<sup>1</sup>*Ioffe Physico-Technical Institute, Saint Petersburg 194021, Russia*

<sup>2</sup>*Department of Physics and Astronomy, University of Waterloo, Waterloo, Ontario N2L 3G1, Canada*  
(Dated: March 28, 2019)

Crystalline semimetals with certain space group symmetries may possess unusual electronic structure topology, distinct from the conventional Weyl and Dirac semimetals. Characteristic property of these materials is the existence of band-touching points with multiple (higher than two-fold) degeneracy and nonzero topological charge. CoSi is a representative of this group of materials exhibiting the so-called “new fermions”. We report on an ab-initio calculation of the electronic structure of CoSi using density functional methods, taking into account the spin-orbit interactions. We demonstrate the existence of band-touching nodes with four- and six-fold degeneracy, located at the  $\Gamma$  and  $R$  points in the first Brillouin zone and near the Fermi energy. We show that these band-touching points carry topological charges of  $\pm 4$  and describe the resulting Fermi arc surface states, connecting the projections of these nodes onto the surface Brillouin zone.

## I. INTRODUCTION

Recent years have witnessed an explosion of interest in semimetals and metals with nontrivial electronic structure topology. The most well-known examples of these are Weyl and Dirac semimetals. The low-energy electronic structure of Weyl semimetals contains an even number of doubly-degenerate band-touching points, carrying topological charges  $\pm 1$ . In certain cases, the Weyl node pairs may exist at the same position in the first Brillouin zone (BZ), producing Dirac points with four-fold degeneracy and zero topological charge. Weyl points with the same topological charge may also merge in crystals with certain symmetries, producing multi-Weyl semimetals.<sup>1</sup>

It has been demonstrated in Ref. 2 that certain space groups allow the existence of nodes with three-, four- (but distinct from Dirac), six-, and eight-fold degeneracy and nonzero topological charge. These band-touching points were called “new fermions” in Ref. 2 in reference to the fact that such structures, unlike Weyl and Dirac nodes, do not exist in the relativistic quantum field theory context, being prohibited by Lorentz invariance.

In this paper we show that CoSi is an example of such a “new fermion” material. CoSi has been studied since the 1960-ies as a thermoelectric material (see review<sup>3</sup>). Early studies demonstrated that its transport properties could be explained if one assumed that the valence and conduction bands overlapped by about 20-40 meV.<sup>3,4</sup> The band dispersions were assumed to be parabolic with the effective masses of electrons and holes of  $2m$  and  $4-6m$ , where  $m$  is the free electron mass.<sup>3,4</sup> However, as will be demonstrated in this work, the real electronic structure of CoSi is significantly more complex.

The crystal structure of CoSi does not contain an inversion center and belongs to the space group 198 ( $P2_13$ ). A simple cubic unit cell contains four formula units and is characterized by the parameters  $a_0 = 4.4445$  Å,  $x_{\text{Co}} = 0.144$ , and  $x_{\text{Si}} = 0.846$ .<sup>3,5</sup> The BZ is a cube with the  $\Gamma$ -point at the center of the cube,  $R$ -points at the

vertices,  $X$  at the centers of the faces and  $M$  at the centers of the edges. Electronic structure calculations using density functional methods were done in Ref. 7 and 8 without taking into account the spin-orbit (SO) coupling and in Ref. 6 with the SO coupling included. Symmetry analysis showed the existence of six-fold degenerate band-touching nodes at the  $R$  point in the BZ and a  $\mathbf{k} \cdot \mathbf{p}$  Hamiltonian, describing the electronic structure in the vicinity of the  $R$  point, was derived.<sup>2,9</sup> The influence of the SO interactions on the electronic structure was discussed in Ref. 6.

The compounds, isostructural to CoSi, are also known. These include, in particular, RhSi. Calculation of the electronic spectrum of this material<sup>10</sup> revealed 4- and 6-fold band degeneracies at the  $\Gamma$  and  $R$  points of the Brillouin zone, respectively. It was also shown that Chern numbers of these nodes are equal to  $\pm 4$ , and the length of each Fermi arc exceeds dimensions of the surface Brillouin zone.

In this paper we present an ab-initio calculation of the electronic structure of CoSi, focusing on the vicinity of the  $\Gamma$  and  $R$  points in the BZ. We show that the band degeneracy nodes at these points carry nontrivial topological charges  $\pm 4$ . We also demonstrate that these nontrivial topological charges lead to the formation of Fermi arc surface states in the two-dimensional surface BZ.

## II. ELECTRONIC STRUCTURE OF COBALT MONOSILICIDE

We calculate the electronic structure of CoSi within generalized gradient approximation (GGA-PBE), taking into account the SO interactions, with the help of the VASP density functional package.<sup>11,12</sup> We used optimized lattice parameters  $a_0 = 4.430$  Å,  $x_{\text{Co}} = 0.145$ , and  $x_{\text{Si}} = 0.843$  (lattice relaxation parameter was 1 meV/Å), which agree well with the experimental values<sup>3,5</sup>. The calculations were performed on  $8 \times 8 \times 8$  Monkhorst-Pack mesh with 350 eV cutoff energy. In agreement with<sup>6-8,13</sup> we find that the states near the Fermi energy are located

near the  $\Gamma$ ,  $M$  and  $R$  points in the BZ (see Fig. 1). We note that the  $G_0W_0$  self-energy correction<sup>14,15</sup> in CoSi<sup>13</sup> shifts the band maximum at the  $M$ -point down in energy by about 0.1 eV. At the same time, the spectrum near the  $\Gamma$  and  $R$  points changes only slightly.

Fig. 2 shows the part of the electronic structure of CoSi near the  $\Gamma$  and  $R$  points in the BZ. It can be shown that the degenerate multiplets at these points arise due to the crystallographic symmetry as well as the time reversal symmetry. Indeed, if SO interactions are neglected, the bands shown in Fig. 2a form a spin-degenerate orbital triplet, transforming under the irreducible representation  $\Gamma_4$  of the little group of the  $\Gamma$  point. SO inter-

action splits the orbital triplet<sup>8</sup> into a doublet  $\bar{\Gamma}_5$  (Weyl node W2 in Fig. 2a) and two degenerate doublets  $\bar{\Gamma}_6$  and  $\bar{\Gamma}_7$  (node W1). Irreducible representations  $\bar{\Gamma}_6$  and  $\bar{\Gamma}_7$  are conjugated. The bases of these representations are transformed into each other under time reversal, guaranteeing their degeneracy. This leads to the appearance of the node W1 at the  $\Gamma$  point, which looks like a pair of Weyl fermions with different Fermi velocities, sharing the same origin in momentum space (this is not an ordinary Dirac point).

At linear order in momentum, the  $\mathbf{k} \cdot \mathbf{p}$  Hamiltonian, which is invariant under transformations of the little group of the  $\Gamma$  point and time reversal takes the form:

$$H_\Gamma = \begin{pmatrix} ak_z & a(k_x - ik_y) & b(e^{\pi i/3}k_x + e^{-5\pi i/6}k_y) & bk_z \\ a(k_x + ik_y) & -ak_z & b(e^{-2\pi i/3}k_x + e^{-5\pi i/6}k_y) & bk_z \\ b^*(e^{-\pi i/3}k_x + e^{5\pi i/6}k_y) & b^*k_z & -ak_z & -a(k_x + ik_y) \\ b^*k_z & b^*(e^{2\pi i/3}k_x + e^{5\pi i/6}k_y) & -a(k_x - ik_y) & ak_z \end{pmatrix}. \quad (1)$$

Here  $\mathbf{k}$  is the wavevector, measured from the  $\Gamma$  point,  $a$  is a real and  $b$  is a complex parameter. When deriving this Hamiltonian, the matrices of the irreducible representations  $\bar{\Gamma}_6$  and  $\bar{\Gamma}_7$  presented in the Bilbao Crystallographic Server<sup>16,17</sup> were used. The energy eigenvalues of this Hamiltonian are given by

$$\epsilon_\pm^2(\mathbf{k}) = \mathbf{k}^2[a^2 + |b|^2 \pm \sqrt{(a^2 + |b|^2)^2 - \det H_\Gamma/\mathbf{k}^4}]. \quad (2)$$

The parameters  $a$  and  $b$  are found by fitting Eq. (2) to the ab-initio spectrum in Fig. 2a. We obtain  $2\pi a/a_0 = 0.56\text{eV}$  and  $2\pi|b|/a_0 = 1.19\text{eV}$ , where  $a_0$  is the size of the elementary cell. The eigenvalues do not depend on  $\arg(b)$ . The fitting near the  $\Gamma$  point is shown in Fig. 3a.

Apart from the W1 and W2 nodes, at the  $\Gamma$ -point, described above, there are several additional doublets, located on high-symmetry axes, which are labelled as W3, W3', and W4 in Fig. 2a. These are ordinary Weyl nodes, which exist due to the lack of inversion symmetry in the crystal structure of CoSi. Here we focus on non-Weyl ("new fermion") nodes at the high-symmetry points in the BZ.

At the  $R$  point in the BZ we find a novel six-fold degenerate node, predicted in Ref. 2. This node is located below the Fermi energy. A little lower in energy we also find a doublet, split from the six-fold degenerate multiplet by the SO interaction. Bands, which form the multiplet, are doubly-degenerate at boundary of the BZ due to the presence of two-fold screw rotations in the crystal symmetry group and time reversal symmetry. In other words, the faces of the cubic unit cell in momentum space form a Weyl nodal surface.<sup>2</sup> Among the irreducible double-valued representations of the little group of  $R$ , the highest-dimensional representation is the real three-dimensional representation  $\bar{R}_7$ . Time reversal symmetry doubles this dimensionality to six<sup>17</sup>. The cor-

responding band Hamiltonian near the  $R$  point to linear order in momentum is given by<sup>2</sup>

$$H_R = \begin{pmatrix} H_{R7}(\tilde{a}) & \tilde{b}H_{R7}(1) \\ \tilde{b}^*H_{R7}(1) & -H_{R7}^*(\tilde{a}) \end{pmatrix}, \quad (3)$$

where

$$H_{R7}(\tilde{a}) = \begin{pmatrix} 0 & \tilde{a}k_x & \tilde{a}^*k_y \\ \tilde{a}^*k_x & 0 & \tilde{a}k_z \\ \tilde{a}k_y & \tilde{a}^*k_z & 0 \end{pmatrix}, \quad (4)$$

and  $\tilde{a}$  and  $\tilde{b}$  are complex parameters. Wave vector is measured from the  $R$  point. Band dispersions may be found from the secular equation

$$\epsilon^6 - 2(|\tilde{a}|^2 + |\tilde{b}|^2)k^2\epsilon^4 + (|\tilde{a}|^2 + |\tilde{b}|^2)^2k^4\epsilon^2 + \det H_R = 0, \quad (5)$$

where  $\det H_R = -(k_x k_y k_z)^2[(\tilde{a} - \tilde{a}^*)^2 + |\tilde{a}|^2 + |\tilde{b}|^2]^2[(\tilde{a} + \tilde{a}^*)^2 + 4|\tilde{b}|^2]$ . The determinant  $\det H_R$ , and thus the roots of the secular equation, depend only on  $|\tilde{a}|$ ,  $|\tilde{b}|$  and  $\arg(\tilde{a})$ , but not on  $\arg(\tilde{b})$ . These parameters are determined by fitting the ab-initio spectrum. We find  $2\pi|\tilde{a}|/a_0 = 0.93\text{eV}$ ,  $2\pi|\tilde{b}|/a_0 = 0.89\text{eV}$ , and  $\arg(\tilde{a}) = 2.42 + m\pi$ , where  $m$  is an integer (the band dispersions are periodic functions of  $\arg(\tilde{a})$  with period  $\pi$  and thus  $\arg(\tilde{a})$  is determined modulo  $\pi$ ). The solutions of equation (5) with these parameters are shown in Fig. 3b. If one of the components of  $\mathbf{k}$  is equal to zero, i.e.  $\mathbf{k}$  is on the cubic BZ boundary,  $\det H_R$  vanishes. In this case, the solutions of Eq. (5) take a simple form

$$\epsilon_0 = 0, \quad \epsilon_\pm = \pm(|\tilde{a}|^2 + |\tilde{b}|^2)k, \quad (6)$$

where all the branches are two-fold degenerate.

The appearance of chiral fermions at high-symmetry points in the BZ, in particular in compounds with space

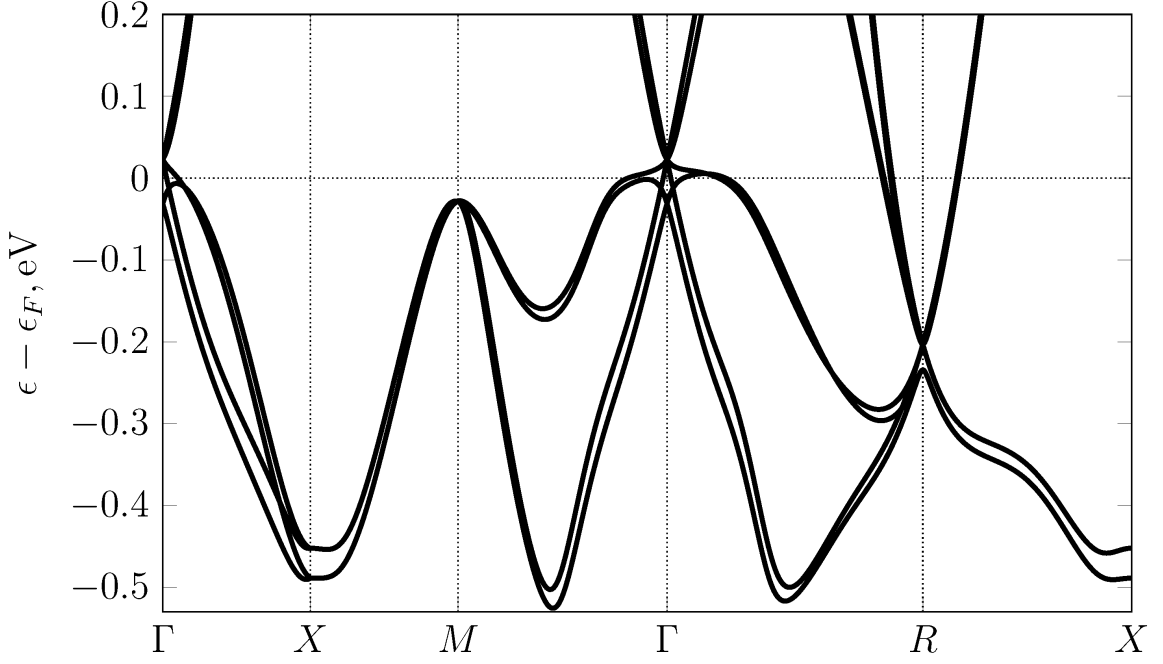


FIG. 1. The band structure of CoSi near the Fermi level calculated with the inclusion of spin-orbit coupling.

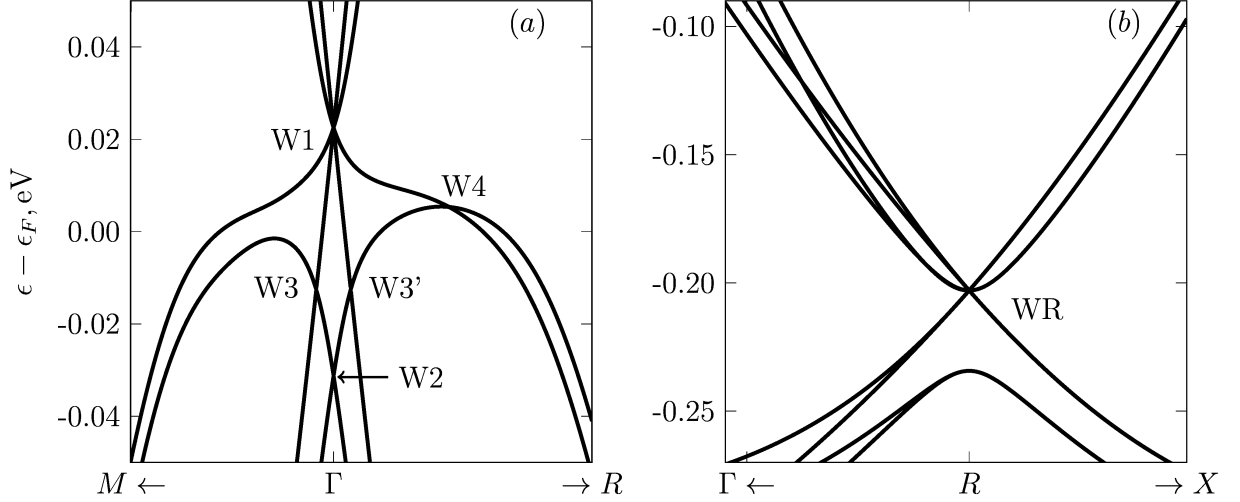


FIG. 2. Band structure of CoSi near  $\Gamma$  (a) and  $R$  (b) points.

group 198, has also been discussed in Ref. 9. It was demonstrated that in the absence of the SO interactions, ignoring the spin and time reversal symmetry, the  $R$  point must host degenerate doublets (“orbital Weyl nodes”), which transform under irreducible representations  $R_1$ ,  $R_2$  or  $R_3$  of the little group at  $R$ . Time reversal symmetry doubles the degeneracy and the number of “orbital Weyl cones”. In other words, the band dispersion in the vicinity of the  $R$  point consists of pairs of “Weyl” cones, distinguished by a “valley” index. In addition, each cone has double spin degeneracy. Once SO interaction is included, it lifts the spin degeneracy,

which results in the following band dispersions near the  $R$  point <sup>9</sup>

$$\epsilon_{1\pm} = \frac{\Delta}{4} \pm vk, \quad (7)$$

and

$$\epsilon_{2\pm} = -\frac{\Delta}{4} \pm \sqrt{\left(\frac{\Delta}{2}\right)^2 + v^2\mathbf{k}^2}, \quad (8)$$

where  $v$  is the band velocity and  $\Delta$  is the strength of the SO interactions. We note that the “valley” degeneracy

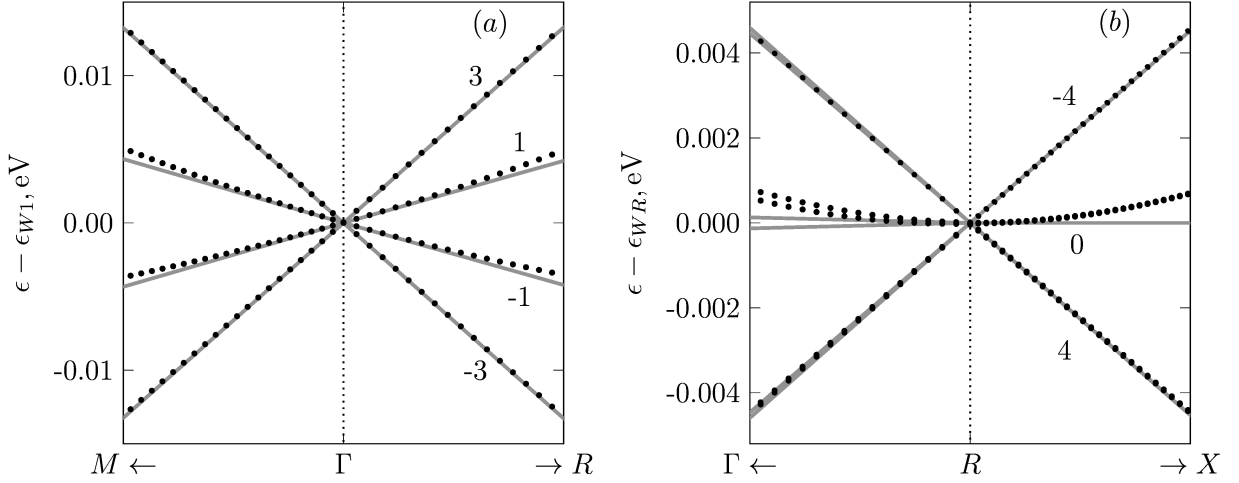


FIG. 3. Energy dispersions of fermions near  $\Gamma$ (a) and  $R$ (b) points. The solid lines represent results of calculations based on the linearized  $\mathbf{k} \cdot \mathbf{p}$  Hamiltonians, the points represent results of *ab initio* calculations of the band structure. Chern numbers are shown close to corresponding bands. Energies are measured from the band crossings.

still remains. Eq. (7) describes massless fermions with linear dispersion, while Eq. (8) — massive Dirac particles. The spectrum branches  $\epsilon_{1\pm}$  and  $\epsilon_{2+}$  are degenerate at the  $R$  point. In a small neighborhood of the  $R$  point, spectrum, described by Eqs. (7) and (8), looks similar to the *ab initio* spectrum, presented on Fig. 2b. Eqs. (5) and (7), (8) complement each other. Dispersion relations, obtained by solving Eq. (5), shown in Fig. 3b, take into account the lifting of band degeneracy away from the  $R$  point, while Eqs. (7) and (8) describe the band splitting, induced by the SO interactions, and parabolicity of some of the branches in the vicinity of the  $R$  point.

### III. CHERN NUMBERS AND FERMION ARCS

One may speak of nontrivial band topology of CoSi if the nodal points, described in the previous section, carry nontrivial topological charges, which in turn may lead to the appearance of Fermi arc surface states. Near the  $\Gamma$  point, the band degeneracy is absent for small but finite wave vectors, and the topological charge is equal to the flux of the Berry curvature  $\mathbf{\Omega}(\mathbf{k})$  through a closed surface in momentum space, enclosing a given degeneracy point. We evaluate the Berry curvature of the band  $n$  as<sup>18–20</sup>

$$\Omega_{\alpha}^{(n)}(\mathbf{k}) = -\epsilon_{\alpha\beta\gamma} \text{Im} \sum_{n' \neq n} \frac{\langle u_n(\mathbf{k}) | H'_{\beta}(\mathbf{k}) | u_{n'}(\mathbf{k}) \rangle \langle u_{n'}(\mathbf{k}) | H'_{\gamma}(\mathbf{k}) | u_n(\mathbf{k}) \rangle}{(\epsilon_n(\mathbf{k}) - \epsilon_{n'}(\mathbf{k}))^2}, \quad (9)$$

where  $|u_n(\mathbf{k})\rangle$  and  $\epsilon_n(\mathbf{k})$  are the eigenstates and energy eigenvalues of the Hamiltonian  $H(\mathbf{k})$ ,  $H'_{\beta}(\mathbf{k}) = \partial H(\mathbf{k}) / \partial k_{\beta}$ , and  $\epsilon_{\alpha\beta\gamma}$  is the fully antisymmetric tensor. One may calculate the Berry curvature using either the first-principles Hamiltonian, or the  $\mathbf{k} \cdot \mathbf{p}$  Hamiltonian (1).

In the former case, the Hamiltonian at an arbitrary point in the BZ is calculated as follows. Using the wavefunctions, obtained in VASP, we utilize the Wannier90 package<sup>21</sup> to construct a tight-binding Hamiltonian. After that, the momentum-space Hamiltonian  $H(\mathbf{k})$  was found by lattice Fourier transform,<sup>22,23</sup> for which we used the TBModels package.<sup>23</sup> As a result of these calculations, we find that at the W1 node, the topological charges of the two pairs of touching bands are equal to  $\pm 3$  and  $\pm 1$ , see Fig. 3a. The W2 node is a standard Weyl node with the Chern number 1. We have also checked our results for the W1 node using the linearized bands Hamiltonian Eq. (1). In this case, the signs of the topological charges depend on the sign of the parameter  $a$  and do not depend on  $\arg(b)$ . They agree with the charges, found from the tight-binding Hamiltonian, when  $a > 0$  is taken.

The above procedure for calculating the topological charges is inapplicable for states near the  $R$  point. This  $k$ -point is located at the crossing of cube faces, where bands are pairwise degenerate. Therefore, the non-Abelian Berry curvature should be used,<sup>19,20</sup> and one can calculate only the total topological charge for a set of degenerate bands, which is enough for our purposes. It is convenient to denote the indices of these bands as  $\{n\}$ . For the calculation of non-Abelian Berry curvature, equation (9) should be corrected by excluding from summation over  $n'$  all bands, degenerate with  $n$ -th one (i.e. by summing over  $n' \notin \{n\}$ ). After that, the non-Abelian Berry curvature for a group of degenerate bands can be obtained by summing up  $\Omega_{\alpha}^{(n)}(\mathbf{k})$  over  $n \in \{n\}$ . As a result we find that, using the first-principles Hamiltonian, the total topological charge of the two linearly dispersing bands is equal to  $-4$  and  $+4$ , respectively (see Fig. 3b). The parabolic bands have zero Chern numbers. The same topological charges were obtained from the low-energy Hamiltonian Eq. (3), if we took  $\arg(\tilde{a}) = 2.42 + m\pi$  with

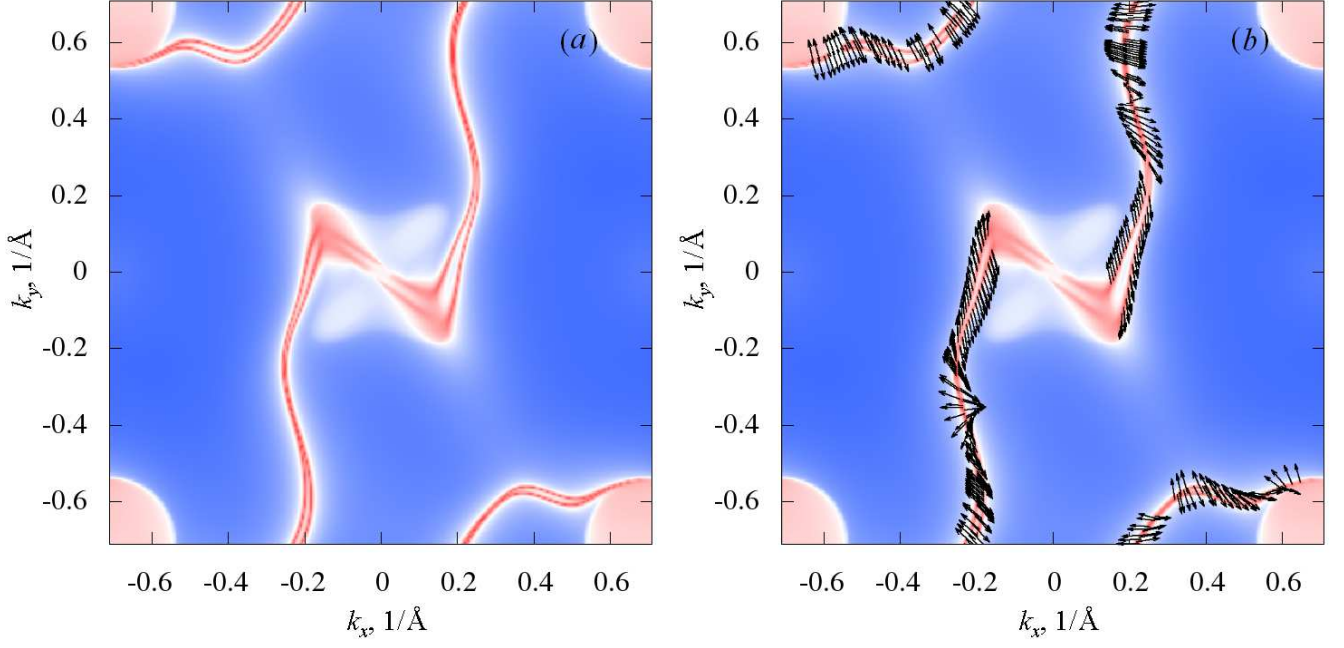


FIG. 4. Distribution of the density of states in the (001) surface Brillouin zone of CoSi slab (a) and the spin texture of surface states (b). The  $\bar{\Gamma}$  point of the bulk Brillouin zone is projected to the square center  $\bar{\Gamma}$ , the points  $R$  and  $M$  are projected to the square vertices  $\bar{M}$ .

odd  $m$ . Even  $m$  result in topological charges of the opposite sign. Topological charges are independent of the phase of the complex parameter  $\tilde{b}$ .

Thus, the total topological charge of the two multiplets at the  $\Gamma$  and  $R$  points is equal to zero, in agreement with the Nielsen-Ninomiya theorem.<sup>24</sup> We note that multiple degeneracy of the bands leads to higher topological charges of some of the bands, in spite of their linear dispersions, as described before in Ref. 2. Similar results for RhSi have been obtained in Ref. 10. This feature distinguishes CoSi from multi-Weyl semimetals, such as SrSi<sub>2</sub>,<sup>25</sup> which possess higher Chern numbers due to band dispersion nonlinearity.

Due to the nonzero topological charges of the nodes at the  $\Gamma$  and  $R$  points, we expect Fermi arc states to exist on certain sample surfaces. We calculated the surface density of states using the WannierTools package.<sup>21,26</sup> Fig. 4a shows the density of states at the Fermi energy in the two-dimensional BZ of the (001) surface. The corresponding picture for the opposite surface of the slab is obtained by the rotation by  $\pi$  around  $k_x$  or  $k_y$  axis. The spin texture of the surface states is shown on the Fig. 4b. One can see that there are four Fermi arcs, which begin and end at the  $\bar{\Gamma}$  and  $\bar{M}$  points, which correspond to the center and the corners of the surface BZ. The bulk multiplets, described above, all have different energy and the Fermi level in undoped CoSi is situated in between them. The deviation of the W1 point from the Fermi energy is small (0.023 eV), while that of the  $R$ -point multiplet is large (-0.2 eV). As a result, the Fermi arcs in Fig. 4 emerge essentially from the center of the surface BZ, but

end at the circles around the  $\bar{M}$  points, which represent projections of the bulk Fermi surface onto the surface BZ. We note four regions of high density of states near the surface BZ center, extended along the  $\bar{\Gamma} - \bar{M}$  directions. These appear due to the presence of two branches of the bulk spectrum near the Fermi energy, which disperse strongly in these directions, see Fig. 2a. Their dispersion in the  $\bar{\Gamma} - X$  directions is significantly weaker, see Fig. 1. Pairs of Fermi arcs pass through these regions. This may be due to nontrivial topology of the W4 nodes, which we have not studied in detail here.

#### IV. CONCLUSIONS

The calculations, reported in this paper, demonstrate that CoSi is a novel type of topological metal, whose electronic structure is significantly different from ordinary Weyl, Dirac and even more exotic multi-Weyl and double-Dirac semimetals. The main new feature of the electronic structure of CoSi is the presence of topologically-nontrivial band-touching nodes with multiple band degeneracy (“new fermions”<sup>2</sup>). The nodes are located at two time reversal invariant points in the BZ and carry nonzero topological charges. The multiplet, located at the  $\Gamma$  point is four-fold degenerate, while the node at the  $R$  point is six-fold degenerate. The two multiplets carry total topological charges of magnitude 4 and opposite signs. Both multiplets are located not far from the Fermi energy and are separated by about 220 meV in energy. The resulting surface states form four Fermi arcs,

which begin and end near the projections of the bulk  $\Gamma$  and  $R$  points onto the surface BZ.

## V. ACKNOWLEDGMENTS

We acknowledge financial support by the Russian Science Foundation, project no. 16-42-01067. AAB was

supported by NSERC of Canada.

- 
- <sup>1</sup> Fang G., Gilbert M.J., Dai X., and Bernevig B.A., Phys. Rev. Lett., **108**, 266802 (2012).
  - <sup>2</sup> Bradlyn B., Cano J., Wang Zh., et al., Science **353**, 558 (2016).
  - <sup>3</sup> Fedorov M.I., Zaitsev V.K., in *CRC Handbook of Thermoelectrics*, ed. by Rowe D.M., CRC Press, Boca Raton, London, New York, Washington, 1995.
  - <sup>4</sup> Asanabe S., Sinoda D., Sasaki Y., Phys. Rev. **134**, A774 (1964).
  - <sup>5</sup> Zelenin L.P., Sidorenko F.A., Geld P.V., Izvestiya Vysshih Uchebnyh Zavedenij. Tsvetnaya Metallurgiya. 7, 146 (1964) (in Russian).
  - <sup>6</sup> Ishii F., Kotaka H., Onishi T., JPS Conf. Proc. **3**, 016019 (2014).
  - <sup>7</sup> Pan Z.J., Zhang L.T., Wu J.S., J. Appl. Phys. **101**, 033715 (2007).
  - <sup>8</sup> Sakai A., Ishii F., Onose Y., et al., J. Phys. Soc. Jap. **76**, 093601 (2007).
  - <sup>9</sup> Manes J.L., Phys. Rev. **B85**, 155118 (2012).
  - <sup>10</sup> Chang G., Xu S.-Y., Wieder B.J., Sanchez D.S., et al., arXiv:1706.04600 (2017).
  - <sup>11</sup> Kresse G., Furthmüller J., Phys. Rev. **B54**, 11169 (1996).
  - <sup>12</sup> Kresse G., Joubert D., Phys. Rev. **B59**, 1758 (1999).
  - <sup>13</sup> Pshenay-Severin D.A., Ivanov Yu.V., Burkov A.T., et al., To be published in Proceedings of Int. Conf. on Thermoelectrics (ICT2017).
  - <sup>14</sup> Shishkin M., Kresse G., Phys. Rev. **B74**, 035101 (2006).
  - <sup>15</sup> Shishkin M., Kresse G., Phys. Rev. **B75**, 235102 (2007).
  - <sup>16</sup> Aroyo M. I., Perez-Mato J. M., Orobengoa D., et al., Bulg. Chem. Commun. **43(2)** 183-197 (2011).
  - <sup>17</sup> Elcoro L., Bradlyn B., Wang Z., Vergniory M.G., et al., arXiv:1706.09272 (2017).
  - <sup>18</sup> Shen Sh.-Q. *Topological insulators. Dirac equation in condensed matters*. Springer, 2012.
  - <sup>19</sup> Baggio M., Niarchos V. and Papadodimas K., J. High Energ. Phys. **2017**, 62 (2017).
  - <sup>20</sup> Resta R. Geometry and topology in electronic structure theory. <http://www-dft.ts.infn.it/~resta/gtse/draft.pdf>
  - <sup>21</sup> Mostofi A.A., Yates J.R., Pizzi G., et al., Comput. Phys. Commun. **185**, 2309 (2014).
  - <sup>22</sup> Wu Q.Sh., Zhang Sh.N., Song H.F., et al., arXiv:1703.07789 (2017).
  - <sup>23</sup> <http://z2pack.ethz.ch/tbmodels>
  - <sup>24</sup> Nielsen H.B., Ninomiya M., Phys. Lett. **B105**, 219 (1981).
  - <sup>25</sup> Huang Sh.-M., Xu S.-Y., Belopolski I., et al., Proc. Nat. Acad. Sci. USA **113**, 1180 (2016).
  - <sup>26</sup> Lopez Sancho M.P., Lopez Sancho J.M., Sancho J. M.L., Rubio J., J. Phys. F: Metal Physics **15**, 851 (1985).